



**HAL**  
open science

## The Northeast Atlantic is running out of excess carbonate in the horizon of cold-water corals communities

Marcos Fontela, Fiz F Perez, Lidia Carracedo, Xosé A. Padín, Antón Velo, Maribel I. García-Ibañez, Pascale Lherminier

### ► To cite this version:

Marcos Fontela, Fiz F Perez, Lidia Carracedo, Xosé A. Padín, Antón Velo, et al.. The Northeast Atlantic is running out of excess carbonate in the horizon of cold-water corals communities. *Scientific Reports*, 2020, 10 (1), 14174 (10p.). 10.1038/s41598-020-71793-2 . hal-04203207

**HAL Id: hal-04203207**

**<https://hal.science/hal-04203207>**

Submitted on 28 Sep 2023

**HAL** is a multi-disciplinary open access archive for the deposit and dissemination of scientific research documents, whether they are published or not. The documents may come from teaching and research institutions in France or abroad, or from public or private research centers.

L'archive ouverte pluridisciplinaire **HAL**, est destinée au dépôt et à la diffusion de documents scientifiques de niveau recherche, publiés ou non, émanant des établissements d'enseignement et de recherche français ou étrangers, des laboratoires publics ou privés.



Distributed under a Creative Commons Attribution 4.0 International License



OPEN

# The Northeast Atlantic is running out of excess carbonate in the horizon of cold-water corals communities

Marcos Fontela<sup>1,2</sup>✉, Fiz F. Pérez<sup>1,2</sup>, Lidia I. Carracedo<sup>3</sup>, Xosé A. Padín<sup>1</sup>, Antón Velo<sup>1</sup>, Maribel I. García-Ibañez<sup>1,4</sup> & Pascale Lherminier<sup>3</sup>

The oceanic uptake of atmospheric carbon dioxide (CO<sub>2</sub>) emitted by human activities alters the seawater carbonate system. Here, the chemical status of the Northeast Atlantic is examined by means of a high-quality database of carbon variables based on the GO-SHIP A25 section (1997–2018). The increase of atmospheric CO<sub>2</sub> leads to an increase in ocean anthropogenic carbon (C<sub>ant</sub>) and a decrease in carbonate that is unequivocal in the upper and mid-layers (0–2,500 m depth). In the mid-layer, the carbonate content in the Northeast Atlantic is maintained by the interplay between the northward spreading of recently conveyed Mediterranean Water with excess of carbonate and the arrival of subpolar-origin waters close to carbonate undersaturation. In this study we show a progression to undersaturation with respect to aragonite that could compromise the conservation of the habitats and ecosystem services developed by benthic marine calcifiers inhabiting that depth-range, such as the cold-water corals (CWC) communities. For each additional ppm in atmospheric pCO<sub>2</sub> the waters surrounding CWC communities lose carbonate at a rate of  $-0.17 \pm 0.02 \mu\text{mol kg}^{-1} \text{ppm}^{-1}$ . The accomplishment of global climate policies to limit global warming below 1.5–2 °C will avoid the exhaustion of excess carbonate in the Northeast Atlantic.

The uptake of anthropogenic CO<sub>2</sub> by the ocean (C<sub>ant</sub>) creates a series of chemical changes known as ocean acidification<sup>1</sup>. The North Atlantic stores the largest amount of C<sub>ant</sub> in the ocean<sup>2,3</sup>, with the Atlantic Meridional Overturning Circulation (AMOC) conveying and exporting acidified C<sub>ant</sub>-loaded waters to the deep ocean<sup>4</sup>. At basin-scale, North Atlantic Ocean acidification is a well-known process<sup>5</sup>, usually reported with pH decrease rates of  $\sim 1\text{--}2 \times 10^{-3}$  pH units yr<sup>-1</sup><sup>6–9</sup>. The reduction in the concentration of carbonate ions ([CO<sub>3</sub><sup>2-</sup>]) is also a consequence of ocean acidification<sup>10</sup>, usually expressed as the change in the calcium carbonate (CaCO<sub>3</sub>) saturation state. The availability of carbonate connects the chemistry of the seawater with the biological activity, since carbonate is used by calcifying organisms to create the different forms of biogenic CaCO<sub>3</sub>: aragonite (corals, pteropods) or calcite (coccolithophores, foraminifera). The difference between the in situ [CO<sub>3</sub><sup>2-</sup>] and the concentration at saturation is the excess of carbonate ( $_{xc}[\text{CO}_3^{2-}]$ )<sup>10,11</sup>. Positive values of  $_{xc}[\text{CO}_3^{2-}]$  indicate supersaturated waters, while negative values indicate undersaturation and the tendency for the biogenic mineral to dissolve<sup>12,13</sup>. Ocean acidification decreases  $_{xc}[\text{CO}_3^{2-}]$ , compromising the fitness of marine calcifiers and even their survival when waters reach negative values of  $_{xc}[\text{CO}_3^{2-}]$ .

Cold-water corals (CWC) with biogenic CaCO<sub>3</sub> skeletons made of aragonite<sup>14</sup> are important ecosystem engineers of deep-sea habitats<sup>15,16</sup>. Ocean acidification is recognized as one of the most challenging threats that CWC will face with global change<sup>17</sup>. At global scale, large CWC reefs are more abundant in the North Atlantic, since the depth at which aragonite becomes susceptible of dissolution is deeper than elsewhere in the world ocean<sup>4,18,19</sup>. In the Northeast Atlantic, the relationship between reefs and hydrography is such that living CWC reefs are located in the potential density range  $27.35 > \sigma_\theta > 27.65 \text{ kg m}^{-3}$ <sup>20</sup>. Recently, several Marine Protected Areas (MPA) have been proposed in European waters based on the presence of *Lophelia pertusa* sp. communities<sup>21,22</sup>. An assessment

<sup>1</sup>Instituto de Investigaciones Marinas, IIM-CSIC, 36208 Vigo, Spain. <sup>2</sup>Centre of Marine Sciences (CCMAR), University of Algarve, 8005-139 Faro, Portugal. <sup>3</sup>Ifremer, Univ. Brest, CNRS, IRD, Laboratoire d'Océanographie Physique et Spatiale (LOPS), IUEM, 29280 Plouzané, France. <sup>4</sup>Centre for Ocean and Atmospheric Sciences, School of Environmental Sciences, University of East Anglia, Norwich, UK. ✉email: mmfontela@ualg.pt

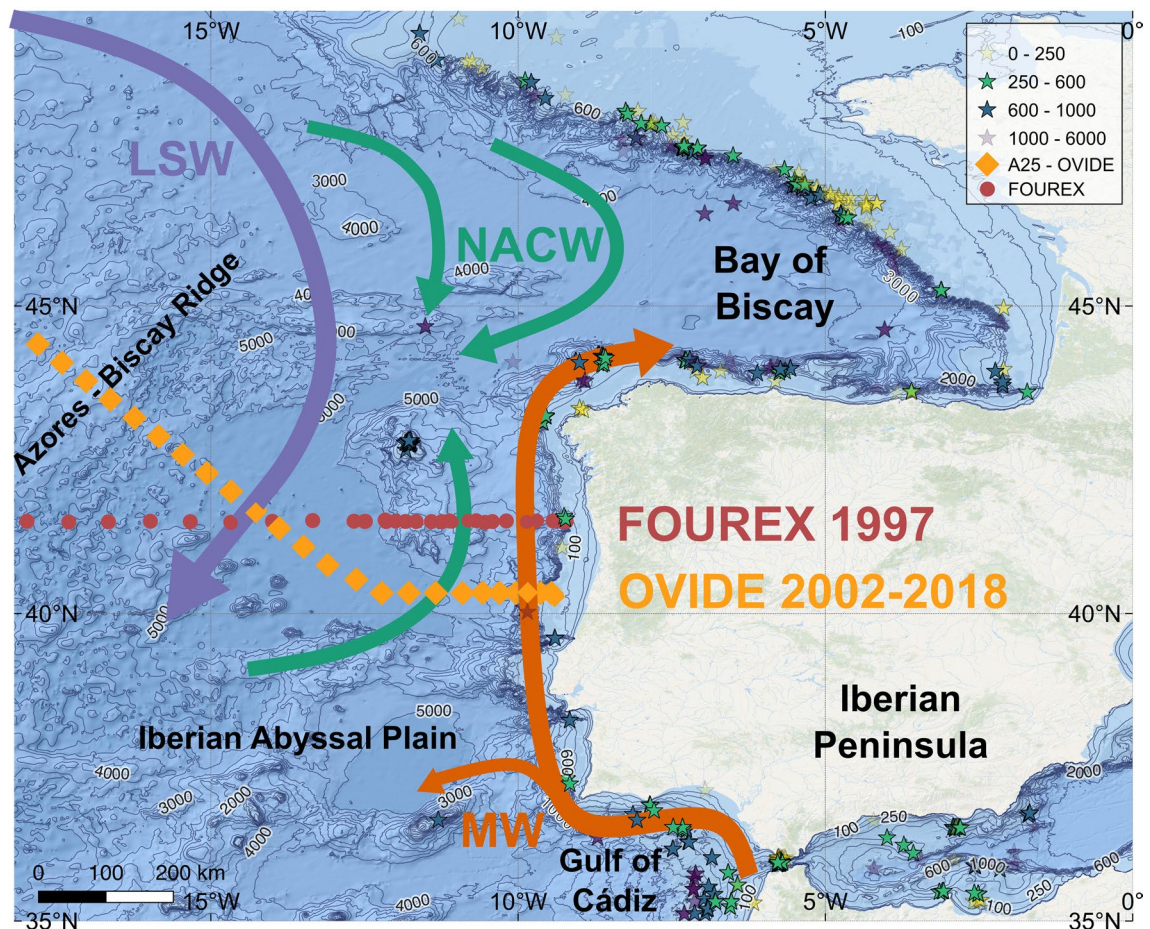


**Figure 1.** Map of the Northeast Atlantic zone of study close to the Iberian Peninsula. The location of the OVIDE (FOUREX) stations used in this study are represented with orange (red) diamonds (circles). The FOUREX section was carried out in 1997 and the OVIDE section has nine repeats, biennially from 2002 to 2018. The Azores-Biscay Ridge is the northern limit of the measurements used in this study. The locations with reported CWC<sup>64</sup> communities where *Lophelia pertusa* is present are represented with stars. The stars are coloured according to the depth of the CWC location (see legend in Figure). A schematic diagram of the large-scale circulation of the main water masses is also shown: North Atlantic Central Water (NACW), Mediterranean Water (MW) and Labrador Sea Water (LSW), adapted from<sup>32,65</sup>.

of the long-term viability of these hotspots of biodiversity and ecosystem services<sup>14</sup> in the context of a changing ocean is therefore necessary.

This study relies on repeated marine chemical surveys across the A25 section of the Global Ocean Ship-Based Hydrographic Investigations Program (GO-SHIP, <https://www.go-ship.org>) to explore the implications of ocean acidification for marine calcifiers from a biogeochemical perspective (Fig. 1). The separation between natural and anthropogenic carbon allows the identification of ocean acidification trends driven by atmospheric CO<sub>2</sub> increase. Although  $x_c[\text{CO}_3^{2-}]$  decrease rates are scarce in the current literature of ocean acidification<sup>23</sup>, the use of this variable is particularly relevant to assess quantitatively the chemical conditions to which marine calcifiers are exposed. The current and future  $x_c[\text{CO}_3^{2-}]$  for the main water masses of the Northeast Atlantic and for the waters where current living communities of CWC exist are reported.

## Results

The vertical distribution of  $x_c[\text{CO}_3^{2-}]$  along the OVIDE cruise section for the year 2018 is shown in Fig. 2. The  $x_c[\text{CO}_3^{2-}]$  values decrease with depth, from supersaturated ( $x_c[\text{CO}_3^{2-}] > 0$ ) surface waters with more than 100  $\mu\text{mol kg}^{-1}$  of  $x_c[\text{CO}_3^{2-}]$ , towards abyssal values of 50  $\mu\text{mol kg}^{-1}$  below saturation ( $x_c[\text{CO}_3^{2-}] < 0$ ). At mid-depths there are larger  $x_c[\text{CO}_3^{2-}]$  values close to the Iberian Peninsula, creating a gradual eastward upward tilt of the isolines. From 3,000 m depth to the bottom, the isolines are horizontal. The isoline of 0  $\mu\text{mol kg}^{-1}$  of  $x_c[\text{CO}_3^{2-}]$ , known as the Aragonite Saturation Horizon (ASH, red dashed line in Fig. 2), is around 2,500 m depth. With respect to the water masses distribution (Table 1), NACW occupies the top layer down to 700 m at the westward end of the section (that is also the northernmost station, Fig. 1) and to around 500 m close to the Iberian Peninsula. Below, MW extends down to about 1,500 m, encompassing entirely the layer where CWC inhabit between 600 and 1,000 m depth range. Beneath MW, LSW reaches 2,500 m. The lower limit of LSW ( $\sigma_2 = 37.00 \text{ kg m}^{-3}$ )

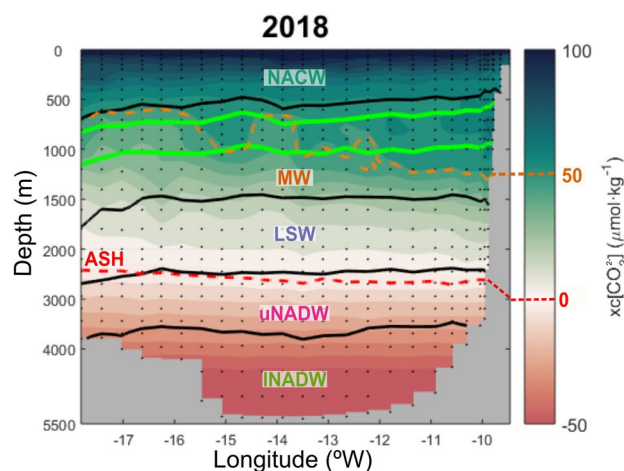


**Figure 2.** Vertical distribution of excess carbonate with respect to aragonite saturation for the year 2018 at the OVIDE section south of Azores-Biscay Ridge. The plot is the vertical distribution (m) between surface and bottom (maximum depth around 5,500 m at longitude 14° W). The orange dash line is the 50  $\mu\text{mol kg}^{-1}$  isoline and the red dash line is the Aragonite Saturation Horizon (ASH, 0  $\mu\text{mol kg}^{-1}$ ). The water masses are separated by black lines of potential density according to the layer separation (acronyms and density values are detailed in Table 1). The layer of living cold-water corals (CWC) is represented within the green isopycnals. Note that the depth-scale is not linear.

Water masses	Acronym	Upper limit ( $\text{kg m}^{-3}$ )	Lower limit ( $\text{kg m}^{-3}$ )	References
North Atlantic Central Water	NACW	Surface	$\sigma_0 = 27.20$	65
Mediterranean Water	MW	$\sigma_0 = 27.20$	$\sigma_1 = 32.35$	
Labrador Sea Water	LSW	$\sigma_1 = 32.35$	$\sigma_2 = 37.00$	27
Upper North Atlantic Deep Water	uNADW	$\sigma_2 = 37.00$	$\sigma_4 = 45.84$	66
Lower North Atlantic Deep Water	INADW	$\sigma_4 = 45.84$	Seafloor	

**Table 1.** Water mass vertical distribution into layers delimited by potential density ( $\sigma_{\text{refpressure}}$ ) isopycnals. Water mass names, acronyms, upper and lower limits of potential density and bibliographic references associated.

and the ASH are pretty similar. The limit between the upper and lower NADW is around 3,800 m depth, where waters are already undersaturated ( $x_{\text{c}}[\text{CO}_3^{2-}] < 0$ ).

The total dissolved inorganic carbon (DIC) mean concentration by water mass (Fig. 3a) shows that the upper layer (NACW) has the lowest values and the bottom layer (INADW) the largest. In the ocean, the amount of DIC usually increases with depth, but in the Northeast Atlantic the MW influence modifies such vertical distribution. The mid-layer MW has a mean DIC concentration higher than the underlying LSW and very similar to uNADW. The concentration of atmospheric  $\text{CO}_2$  for the period 1997–2018 increased from 364 to 409 ppm (Fig. 3), with an annual mean increase larger than 2 ppm  $\text{yr}^{-1}$ . For DIC, the increase trend with increasing atmospheric  $\text{CO}_2$  concentration is only found in the uppermost water mass, NACW (results of statistical hypothesis test in Supplementary information Table S1).

DIC includes the natural ( $\text{DIC}_{\text{nat}}$ ) and the anthropogenic ( $C_{\text{ant}}$ ) components.  $\text{DIC}_{\text{nat}}$  (Fig. 3b) shows a more monotonous increase from surface to bottom than DIC, although  $\text{DIC}_{\text{nat}}$  concentrations for MW and LSW are very similar. In addition, contrary to the total DIC,  $\text{DIC}_{\text{nat}}$  does not show a trend with increasing atmospheric  $\text{CO}_2$  in any layer. When  $C_{\text{ant}}$  is analyzed (Fig. 3c), its vertical distribution shows that the surface-most NACW has the highest concentration, which decreases until values slightly above zero in the deeper layers. The increase in  $C_{\text{ant}}$  with increasing atmospheric  $\text{CO}_2$  is unequivocal in the upper and mid-layers (Supplementary information Table S1), but not for NADW layers. As expected from direct air-sea  $\text{CO}_2$  exchange, the largest increase in  $C_{\text{ant}}$  occurs in the surface-most NACW layer ( $0.38 \pm 0.02 \mu\text{mol kg}^{-1} \text{ppm}^{-1}$ ), with concentrations exceeding  $60 \mu\text{mol kg}^{-1}$  by the end of the observational period. MW and LSW mid-layers show rather similar increase in  $C_{\text{ant}}$  concentration rates ( $0.15 \pm 0.02 \mu\text{mol kg}^{-1} \text{ppm}^{-1}$  and  $0.09 \pm 0.01 \mu\text{mol kg}^{-1} \text{ppm}^{-1}$ , respectively). Note that when time (in years) is used as dependent variable (Fig. S1), the results remain consistent. The vertical distributions of DIC,  $C_{\text{ant}}$  and  $\text{DIC}_{\text{nat}}$  along the OVIDE cruise section for the year 2018 are shown in Fig. S2.

The vertical distributions of total alkalinity (TA) and TA normalized by salinity ( $S = 35$ ) along the OVIDE cruise section for the year 2018 are shown in Figure S3. The TA mean concentration by water mass does not show

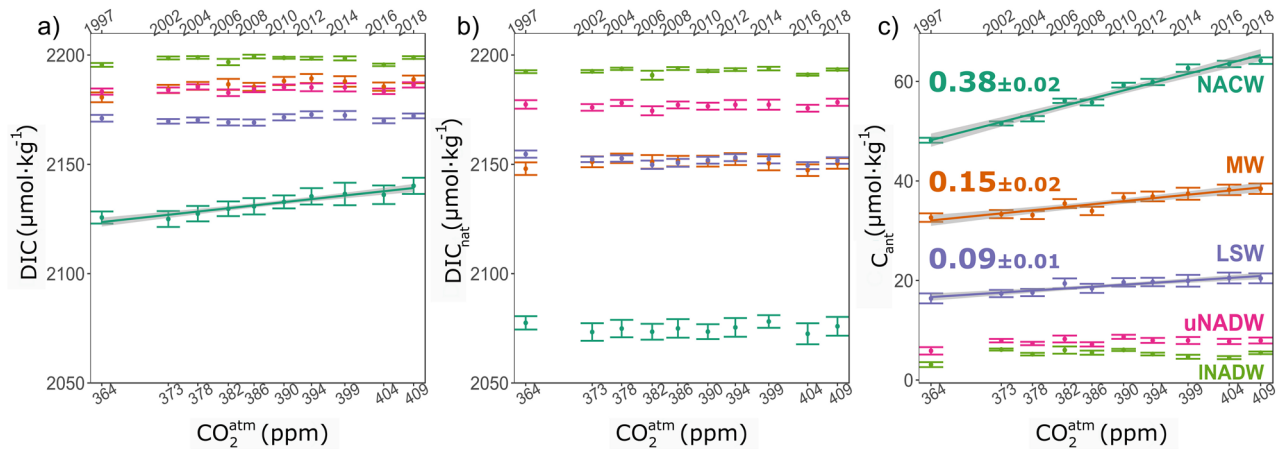


**Figure 3.** Mean layer concentration trends of dissolved inorganic carbon components in Northeast Atlantic water masses versus atmospheric  $\text{CO}_2$  concentration. Mean layer (a) total DIC concentration ( $\mu\text{mol kg}^{-1}$ ) and its separation into (b) natural ( $\text{DIC}_{\text{nat}}$ ,  $\mu\text{mol kg}^{-1}$ ) and (c) anthropogenic ( $C_{\text{ant}}$ ,  $\mu\text{mol kg}^{-1}$ ) components versus atmospheric  $\text{CO}_2$  concentration (ppm) for the main water masses in the Northeast Atlantic: NACW (cyan), MW (orange), LSW (purple) and upper and lower NADW (pink and light green). Only linear trends ( $\mu\text{mol kg}^{-1} \text{ppm}^{-1}$ ) with a statistical  $p$ -value  $< 0.001$  (Supplementary Information Table S1) have been depicted, and the grey shading accounts for the trend errors. Uncertainties in the mean properties are two times the standard error of the mean (i.e., 95% confidence interval). The year of the cruise is represented in the upper x-axis.

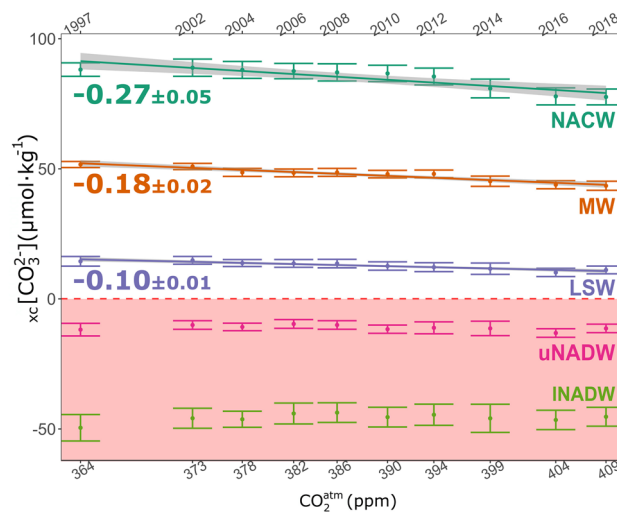


**Figure 4.** Mean water mass  $x_c[\text{CO}_3^{2-}]$  ( $\mu\text{mol kg}^{-1}$ ) versus atmospheric  $\text{CO}_2$  concentration (ppm) in the Northeast Atlantic: NACW (cyan), MW (orange), LSW (purple) and upper and lower NADW (pink and light green). Only linear trends ( $\mu\text{mol kg}^{-1} \text{ppm}^{-1}$ ) with a statistical  $p$ -value  $< 0.001$  have been depicted (Supplementary Information Table S1), and the grey shading accounts for the trend errors. Uncertainties in the mean properties are two times the standard error of the mean (i.e., 95% confidence interval). The year of the cruise is represented in the upper x-axis. The light red zone below the limit of  $0 x_c[\text{CO}_3^{2-}]$  represents undersaturated waters with respect to aragonite.

any trend with increasing atmospheric  $\text{CO}_2$  concentration (Fig. S3a). The variation of TA is highly correlated with salinity. The distribution of TA normalized (Fig. S3b) shows a steady increase towards the bottom that is due to  $\text{CaCO}_3$  dissolution but has a very low effect on  $[\text{CO}_3^{2-}]^{24}$ .

The trends of the mean  $x_c[\text{CO}_3^{2-}]$  by water mass and associated uncertainties with respect to the atmospheric  $\text{CO}_2$  concentration for 1997–2018 are represented in Fig. 4. The pattern of  $x_c[\text{CO}_3^{2-}]$  values between water masses follows a vertical distribution, with positive  $x_c[\text{CO}_3^{2-}]$  values at the surface and negative values in deep waters. The  $x_c[\text{CO}_3^{2-}]$  decreases with the excess of atmospheric  $\text{CO}_2$  in the upper (NACW,  $-0.27 \pm 0.05 \mu\text{mol kg}^{-1} \text{ppm}^{-1}$ ) and mid-layers (MW  $-0.18 \pm 0.02 \mu\text{mol kg}^{-1} \text{ppm}^{-1}$ , and LSW  $-0.10 \pm 0.01 \mu\text{mol kg}^{-1} \text{ppm}^{-1}$ ) of the Northeast Atlantic. Such decrease in  $x_c[\text{CO}_3^{2-}]$  does not exist in the two layers of NADW ( $p$ -values of 0.13 and 0.29 for upper and lower NADW, respectively). The rate of decrease in  $x_c[\text{CO}_3^{2-}]$  is almost three times larger at surface than in LSW, with its physicochemical properties and its position in the water column making LSW to be close

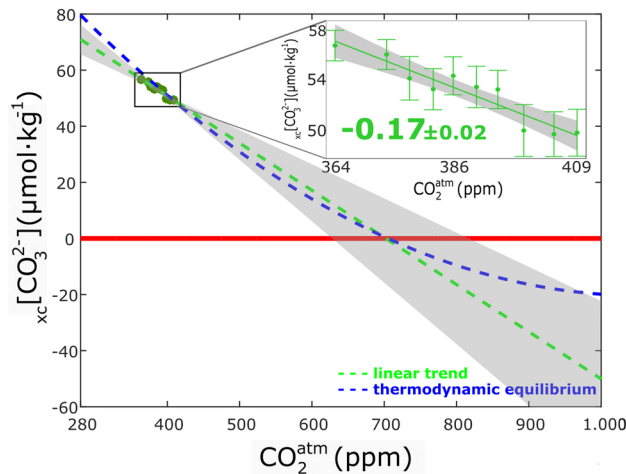


**Figure 5.** Mean  $_{xc}[\text{CO}_3^{2-}]$  ( $\mu\text{mol kg}^{-1}$ ) versus atmospheric  $\text{CO}_2$  concentration (ppm) for the living cold-water coral (CWC) layer ( $\sigma_0 = 27.35\text{--}27.65 \text{ kg m}^{-3}$ ) observed (inset) and predicted. The inset shows the observed measurements and the grey shading accounts for the trend errors. The linear trend in the inset (green line,  $\mu\text{mol kg}^{-1} \text{ ppm}^{-1}$ ) has a statistical  $p$ -value =  $4.3 \times 10^{-5}$ . In the inset, the uncertainties in the mean properties are two times the standard error of the mean (i.e., 95% confidence interval), and the year of the cruise is represented in the upper x-axis. The predictions (dashed lines) are based on the linear rate of decrease for the observational period (green) and on the thermodynamic equilibrium trend (blue, Orr et al.<sup>10</sup>).

to the limit of no excess. If these trends persist in time, LSW will become undersaturated in the Northeast Atlantic when a concentration of  $514 \pm 31$  ppm of atmospheric  $\text{CO}_2$  is reached.

In the depth range of living CWC, the change in  $_{xc}[\text{CO}_3^{2-}]$  with increasing atmospheric  $\text{CO}_2$  shows a decrease from 56 to less than  $50 \mu\text{mol kg}^{-1}$  during the observing time frame (inset in Fig. 5). The rate of decrease is  $-0.17 \pm 0.02 \mu\text{mol kg}^{-1} \text{ ppm}^{-1}$  ( $p$ -value =  $4.3 \times 10^{-5}$ ). Conserving this linear trend, the current layer of living CWC in the Northeast Atlantic would then be in undersaturated waters at a concentration of  $702 \pm 53$  ppm of atmospheric  $\text{CO}_2$  (Fig. 5). The nonlinearity between ocean carbon variables requires a thermodynamical approach to infer distant projections<sup>10</sup>. However, within a thermodynamic equilibrium, the layer of living CWC approximately follows the linear trend (Fig. 5). The large loss of linearity occurs below the undersaturation level ( $_{xc}[\text{CO}_3^{2-}] < 0$ ), so the linear trend is a valid approach for the study purposes.

## Discussion

In the huge pool of inorganic carbon existing in the ocean, the anthropogenic component represents a relatively small fraction of it (<4%)<sup>2</sup>. Current anthropogenic perturbation in NACW layer (<600 m depth, approximately) is large enough to be detected in the DIC pool within a 21-year timespan (1997–2018) (Fig. 3a). The detection of trends in DIC, however, may require longer time series if the measurements are not normalized by salinity<sup>6</sup> or alkalinity. In the Northeast Atlantic, the increase in DIC is not mediated by a change in total alkalinity (Fig. S3). And even without salinity normalization, the large anthropogenic perturbation, combined with the fact that all measurements were made in the same season (summer), favors the detection of trends<sup>5</sup>. This 21-year timescale agrees well with the 14-year period required to detect the emergence of the anthropogenic signal from natural variability in another carbon variable, the surface pH<sup>25</sup>. In contrast, the natural DIC shows no change at any layer (Fig. 3b, Supplementary Information Table S1) suggesting that, within this approach, we cannot discard the steady-state of the natural carbon cycle in the Northeast Atlantic. Nevertheless, the capability of current anthropogenic carbon methods to discern changes in the natural DIC is still a debated subject<sup>26</sup> that is out of the scope of the present study. For the  $C_{\text{ant}}$ , increasing trends are unequivocally observed not only in the upper NACW layer but also in the mid-layer water masses, i.e., until 2,500 m depth. There is a consistent increase in  $C_{\text{ant}}$  in the upper and mid-layers of the Northeast Atlantic that responds to the atmospheric  $\text{CO}_2$  increase over time. These results agree, and update by more than a decade, the previously reported  $C_{\text{ant}}$  trends in the Northeast Atlantic<sup>27</sup>. The  $C_{\text{ant}}$  increase in the NACW layer is among the largest trends reported in the literature<sup>9,27</sup>, in agreement with the view that the subtropical areas are the places where the upper water masses increase its  $C_{\text{ant}}$  burden<sup>3,28–30</sup>. South of the study zone, in the Gulf of Cadiz region (Fig. 2), the downwelling of central waters with high  $C_{\text{ant}}$  concentrations and the subsequent formation of MW exports  $C_{\text{ant}}$  to the Northeast Atlantic<sup>31</sup>. This convection of the anthropic signal at mid-depths is then advected, spreading acidified waters to the North Atlantic. Although the anthropogenic influence has already reached the old water masses (NADW) of the Iberian Abyssal Plain, a longer monitoring period is required to identify it. In summary, the combination of the natural component of DIC in steady-state with the unequivocal trends for  $C_{\text{ant}}$  in NACW, MW and LSW, makes it reasonable to assume that the existence of perturbations in other marine carbonate system variables are also produced by human influence, as seen for pH,  $\text{CO}_3$  (Fig. S4, Table S1) and  $_{xc}[\text{CO}_3^{2-}]$  (Fig. 4). The latter is the variable that we are going to consider hereafter.

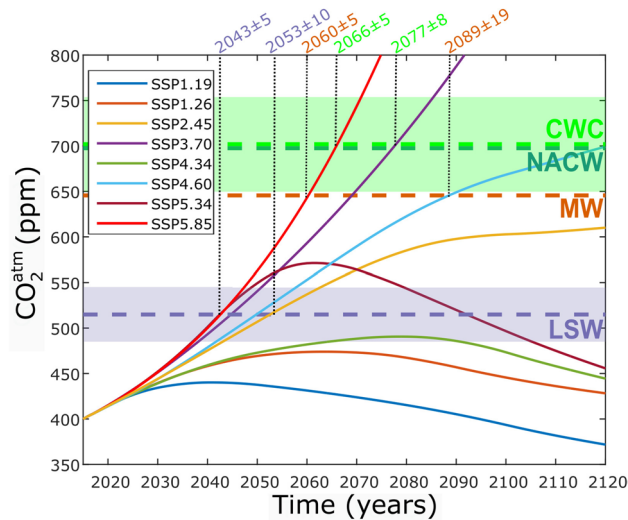


**Figure 6.** Projections of atmospheric CO<sub>2</sub> concentration (ppm) versus time (years) as modelled by the eight Shared Socioeconomic pathways (SSPs) considered. Atmospheric CO<sub>2</sub> data from<sup>39</sup>. The horizontal dashed lines are the predicted atmospheric concentration at the moment of undersaturation for each layer. The predicted uncertainty for the LSW and CWC layers is the 95% confidence interval at the moment of undersaturation for the projected mean properties linear trends; and it is represented with the light-colored horizontal band. For specific pathways, the expected year of reaching undersaturation along with their uncertainty is included in the upper axis.

$_{\text{cc}}[\text{CO}_3^{2-}]$  decreases with depth due to solubility (high pressure and low temperature increases aragonite solubility). The anthropogenic decline of  $_{\text{cc}}[\text{CO}_3^{2-}]$  exists in all the supersaturated water masses, that is, NACW, MW and LSW. The decline is happening three times faster in NACW than in LSW, as expected from the atmospheric source of the driver for ocean acidification (atmospheric CO<sub>2</sub>) and the age of these water masses<sup>9</sup>. The relatively young and recently formed NACW has the largest trend, whereas LSW, ventilated in western subpolar latitudes, reaches the Northeast Atlantic basin with a greater mean age and hence has the lowest trend among the acidified water masses. MW, formed at the southeast of the Iberian Peninsula (Gulf of Cadiz, Fig. 2) by mixing of NACW, Mediterranean Outflow Water (MOW) and a diluted form of Antarctic Intermediate Water<sup>32,33</sup>, shows intermediate trends. At the latitudes of the measurements, the layer with living CWC is comprised within the MW layer, between 600 and 1,000 m depth. Therefore, the living CWC are in waters with excess of available carbonate, in agreement with the idea that suitable habitats for CWC development are supersaturated for aragonite<sup>18</sup>. MOW contributes for around a third (~34%) in the composition of MW<sup>32</sup>. Due its intrinsic properties of high salinity and alkalinity<sup>34,35</sup>, MW is therefore crucial to keep the Northeast Atlantic CWC in chemically optimal waters. In the Gulf of Cadiz, the ocean acidification rates in MW are relatively high<sup>36</sup>. Currently, living CWC are located between the fast-acidifying surface waters from above and the rising ASH from below. A potential reduction in MOW by global change<sup>37</sup> would involve a greater influence of subpolar origin waters that could accelerate the exhaustion of excess carbonate in the Northeast Atlantic.

Reaching undersaturation for aragonite in the upper and mid-layers of the Northeast Atlantic would take less than a century in worst scenarios (SSP5.85, SSP4.60 and SSP3.70, Fig. 6). Fossil-fueled development pathway SSP5.85 is similar to that projected by the previous IPCC business-as-usual scenario (RCP8.5)<sup>38</sup>. The scenarios that best represent the limitation of global warming to 1.5 or 2 °C of the Paris Agreement are the SSP1-19 and the SSP1-26 respectively<sup>39</sup>. For both scenarios, the decline of  $_{\text{cc}}[\text{CO}_3^{2-}]$  will not reach undersaturation values not even in LSW layer (Fig. 6). Therefore, if the CO<sub>2</sub> emission targets for limiting global warming to 1.5 or 2 °C are accomplished, the Northeast Atlantic will remain in chemically optimal conditions for CWC communities the following century. However, if the atmospheric CO<sub>2</sub> concentration reached 700 ppm, then the living CWC communities in the Northeast Atlantic would be exposed to waters that are chemically hostile to their carbonate structures. Our projection based in measurements is in agreement with previous model forecasts<sup>10,18</sup>.

Many species of benthic calcifiers, even CWC other than *Lophelia pertusa*, inhabit undersaturated seawaters<sup>40,41</sup>. Although living CWC can have net calcification in undersaturated conditions<sup>42,43</sup>, they do it at expenses of stored energy reserves<sup>44</sup>. Three-dimensional CWC reefs structures are composed by an important fraction (>70%) of dead corals framework<sup>45</sup>. In contrast to the living CWC, the dissolution of the dead skeletons is a predicted chemical reaction<sup>46</sup> because the skeletons have no capacity to cope with dissolution. The net dissolution will be directly proportional to the time CWC remain in undersaturated waters and that could happen within a century if the Paris Agreement is not accomplished. To the best of our knowledge, there are no long-term in situ experiments that confirm net dissolution of dead CWC framework available at this time. However, the combination of bioerosion proceeding faster in substrates weakened by ocean acidification<sup>47</sup> with the close relationship between carbonate availability and the location of healthy CWC communities<sup>4,18,19</sup> suggests that CWC development might be compromised. Furthermore, the decrease in available carbonate saturation

level may combine with, and potentially exacerbated by, other climate change pressures such as warming and deoxygenation<sup>48,49</sup>.

## Conclusions

The uptake of anthropogenic carbon from the atmosphere is unequivocally decreasing the amount of carbonate available for marine calcifiers in the upper (NACW) and intermediate water masses (MW and LSW) of the Northeast Atlantic Ocean. The northward spreading of MW plays a key role in limiting the arrival of subpolar-origin waters with low excess of carbonate available. The chemical conditions that made the Northeast Atlantic a region favorable for CWC development in preindustrial time are changing fast due to ocean acidification. Currently, provided the water masses contribution remain the same, living CWC would inhabit undersaturated waters when the atmospheric CO<sub>2</sub> concentration reaches 702 ± 57 ppm. If greenhouse gas emissions maintain the path of fossil-fuel development, the running out of excess carbonate in the Northeast Atlantic will take place during this century. The efficiency of high seas Marine Protected Areas (MPA) created for the long-term conservation of CWC and their associated ecosystems is ultimately associated with the accomplishment of the Paris Agreement and the limitation of global warming below 2 °C.

## Materials and methods

Two-decades of ocean acidification trends across the whole water column of the Northeast Atlantic are evaluated by means of high-quality CO<sub>2</sub> measurements. The observations came from ten hydrographic cruises across the Iberian Abyssal Plain between 1997 and 2018 (Fig. 2): the 1997 FOUREX cruise (CLIVAR Carbon Hydrographic Data Office site, [https://cchdo.ucsd.edu/cruise/74DI230\\_1](https://cchdo.ucsd.edu/cruise/74DI230_1)) and 9 repeats of the OVIDE section (OVIDE group, 2020). They are almost evenly spaced in time since all cruises except the first one belong to the OVIDE sampling program, a high-resolution hydrographic survey that has been carried out every other year during spring–summer since 2002 (<https://www.umr-lops.fr/en/Projets/Projets-actifs/OVIDE>). The assembled high-quality CO<sub>2</sub> system database between the Azores Biscay Ridge (45° N, 18° W) and the Iberian Peninsula therefore spans 21 years (1997–2018; Fig. 2) and the whole-water column (Fig. 1). Note the cruise track is identical for the nine repetitions of the OVIDE section, but it is slightly southern for the 1997 cruise. Both coast-to-coast hydrographic sections belong to GO-SHIP (Global Ocean Ship-Based Hydrographic Investigations Program), which is part of the global ocean/climate observing systems (GOOS/GCOS)<sup>50</sup>. Note here we are analyzing their easternmost part (< 18° W) exclusively.

**Measured carbon variables: pH and total alkalinity.** In this study, the carbon analysis for all the hydrographic data involved followed the same analytical methodology and were in situ calibrated against Certified Reference Materials (CRMs).

pH was determined with a spectrophotometric method<sup>51</sup>. The protocols of measurements developed and followed during the cruises, including periodical CRM checks, allowed to achieve an internal consistency and reproducibility of ± 0.0014 pH units<sup>9,27</sup>. The large amount of measurements from the deeper waters sampled at the Iberian Abyssal Plain (n = 1,633) show a very low standard deviation (7.9146 ± 0.0006 pH at in situ conditions of temperature and pressure in the total scale), which is a useful indicator of consistency and reproducibility since these old waters are expected to be in near steady state<sup>9</sup>. Total alkalinity (TA) was analyzed by single point titration<sup>52</sup> and calibrated with CRM with a measurement precision of ± 2 μmol kg<sup>-1</sup>. Over 3,200 samples of TA were analyzed for this study, with around three hundred per cruise for the stations shown in Fig. 2. The amount of total alkalinity measurements with WOCE flags values different from “Acceptable” is less than 1%. The datasets were subject to primary and secondary quality control procedures<sup>53</sup> consistent with the GLODAP data products<sup>54,55</sup> and neither carbon related variables (pH and total alkalinity) nor oxygen have been modified at the secondary quality control procedure<sup>55</sup>. Then, results are supported by high-quality and low-uncertainty carbon measurements spanning 21 years.

**Computed carbon variables.** Concentrations of dissolved inorganic carbon (DIC) and in situ carbonate ions ([CO<sub>3</sub><sup>2-</sup>]<sub>is</sub>) were calculated with the CO2SYS toolbox<sup>56</sup> using the acid dissociation constants of Mehrbach et al.<sup>57</sup> refitted by Dickson and Millero<sup>58</sup>, and the aragonite solubility of Mucci<sup>59</sup>. The uncertainty in the concentrations is ± 4.6 μmol kg<sup>-1</sup> and ± 3.7 μmol kg<sup>-1</sup> for DIC and [CO<sub>3</sub><sup>2-</sup>]<sub>is</sub>, respectively<sup>60</sup>.

The in situ degree of aragonite saturation (Ω<sub>Arg</sub>) is the product of the ion concentrations of calcium ([Ca<sup>2+</sup>]) and carbonate ([CO<sub>3</sub><sup>2-</sup>]) divided by the aragonite solubility product (K<sub>Arg</sub>) at in situ conditions (subscript “<sub>is</sub>”) of temperature, salinity, and pressure<sup>12</sup>. Following the Ω<sub>Arg</sub> definition:

$$\Omega_{\text{Arg}} = \frac{[\text{Ca}^{2+}] [\text{CO}_3^{2-}]_{\text{is}}}{K_{\text{Arg}}}, \quad (1)$$

we can infer [CO<sub>3</sub><sup>2-</sup>] at saturation (i.e., when Ω<sub>Arg</sub> equals one):

$$[\text{CO}_3^{2-}]_{\text{sat}(\Omega_{\text{Arg}}=1)} = \frac{K_{\text{Arg}}}{[\text{Ca}^{2+}]}, \quad (2)$$

where the concentration of the conservative ion [Ca<sup>2+</sup>] is determined only by salinity<sup>61</sup>. Both K<sub>Arg</sub> and [Ca<sup>2+</sup>] were calculated with the CO2SYS toolbox<sup>56</sup>. The difference between [CO<sub>3</sub><sup>2-</sup>]<sub>is</sub> and [CO<sub>3</sub><sup>2-</sup>]<sub>sat(Ω<sub>Arg</sub>=1)}</sub> (Eq. 2) is the excess of carbonate ion concentration over aragonite saturation: <sub>xc</sub>[CO<sub>3</sub><sup>2-</sup>]<sup>4,11</sup>. Note that an alternative estimate is the <sub>xc</sub>[CO<sub>3</sub><sup>2-</sup>] over calcite saturation, computed with the degree of calcite saturation (Ω<sub>Calcite</sub>). Since calcite is



more resistant to dissolution than aragonite<sup>11</sup>, calcifying organisms that form their structures with calcite will be less affected by ocean acidification at shorter time-scales<sup>62</sup>. Therefore, in this work, we refer exclusively to excess carbonate and the saturation state with respect to aragonite.

Finally, anthropogenic carbon ( $C_{\text{ant}}$ ) was estimated with the biogeochemical back-calculation  $\phi C_T$  method<sup>63</sup>, which has an overall uncertainty of  $\pm 5.2 \mu\text{mol kg}^{-1}$ . The natural fraction in the total DIC ( $\text{DIC}_{\text{nat}}$ ) is the difference between DIC and  $C_{\text{ant}}$ .

**Layer separation.** The whole-water column was separated following a vertical water mass distribution into five layers delimited by potential density ( $\sigma_{\text{refpressure}}$ ) isopycnals (Table 1, Fig. 1), following previous studies in the area<sup>8,27</sup>. The reference pressure level for the isopycnals (refpressure) varies among 0, 1, 2 and 4 ( $\times 10^3$  dbar).

In addition, we also delimited the range of water column where living CWC exist in the Northeast Atlantic<sup>20</sup>, i.e.  $27.35 \leq \sigma_0 \leq 27.65 \text{ kg m}^{-3}$  (Fig. 1).

For each layer, the mean property concentrations ( $x_c[\text{CO}_3^{2-}]$ , DIC,  $\text{DIC}_{\text{nat}}$ ,  $C_{\text{ant}}$ , TA,  $\text{pH}_{\text{is}}$ , T and  $[\text{CO}_3^{2-}]_{\text{is}}$ ) were based on interpolated bottle data at dbar resolution. Interpolation was done on an area-weighted basis, considering the thickness of the layer and the distance between measurements<sup>9</sup>. The mean properties are represented along with the 95% confidence interval (error bars are two times the standard error of the mean,  $2x(\text{std}/\sqrt{n})$ ; where  $n$  is the number of bottle measurements in that layer and cruise, Figs. 3, 4, 5).

**Atmospheric CO<sub>2</sub>: past concentrations and shared socioeconomic pathways projections.** In this study we contrasted the anthropogenic changes in the ocean carbon cycle with respect to its main driver, the atmospheric CO<sub>2</sub> concentration, in contrast to previous studies in the region using time as dependent variable<sup>8,9</sup>. Note that this methodology develops rates with respect to atmospheric CO<sub>2</sub> rather than time, so the units of the rates are  $\mu\text{mol kg}^{-1} \text{ ppm}^{-1}$ . Atmospheric CO<sub>2</sub> concentration is a more meaningful variable than time, since it allows to make projections directly based on greenhouse gas concentrations resulting from different policy decisions and socioeconomic pathways. Past atmospheric CO<sub>2</sub> concentrations were taken from the Mauna Loa database (<https://www.esrl.noaa.gov/gmd/ccgg/trends/>) [last time accessed: 28/12/2019]. In this study we used the mean annual concentration of CO<sub>2</sub> (in parts per million of volume, p.p.m.) for the year of the cruise. Shared Socioeconomic Pathways (SSP) are climate scenario frameworks that take into account a wide range of socioeconomic futures and policy decisions<sup>38</sup>. Atmospheric CO<sub>2</sub> concentrations for eight representative SSP scenarios belonging to the Coupled Model Intercomparison Project phase 6 (CMIP6) were downloaded from <https://greenhousegases.science.unimelb.edu.au> [last time accessed: 28/12/2019]<sup>39</sup>. This data is used in the atmospheric CO<sub>2</sub> concentration projections.

## Data availability

Data were collected and made publicly available by the International Global Ship-based Hydrographic Investigations Program (GO-SHIP; <https://www.go-ship.org/>) and the national programs that contribute to it. Global Distribution of Cold-water Corals version 5.0 (June 2018) is distributed under UNEP-WCMC's General Data License (excluding WDPA). URL: <https://data.unep-wcmc.org/datasets/3>.

Received: 6 March 2020; Accepted: 21 August 2020

Published online: 07 September 2020

## References

- Caldeira, K. & Wickett, M. E. Anthropogenic carbon and ocean pH. *Nature* **425**, 365 (2003).
- Khatiwal, S. *et al.* Global ocean storage of anthropogenic carbon. *Biogeosciences* **10**, 2169–2191 (2013).
- Gruber, N. *et al.* The oceanic sink for anthropogenic CO<sub>2</sub> from 1994 to 2007. *Science* **363**, 1193–1199 (2019).
- Perez, F. F. *et al.* Meridional overturning circulation conveys fast acidification to the deep Atlantic Ocean. *Nature* **554**, 515–518 (2018).
- Bates, N. R. *et al.* A time-series view of changing surface ocean chemistry due to ocean uptake of anthropogenic CO<sub>2</sub> and ocean acidification. *Oceanography* <https://doi.org/10.5670/oceanog.2014.16> (2014).
- Santana-Casiano, J. M., González-Dávila, M., Rueda, M. J., Llinás, O. & González-Dávila, E. F. The interannual variability of oceanic CO<sub>2</sub> parameters in the northeast Atlantic subtropical gyre at the ESTOC site. *Glob. Biogeochem. Cycles* **21**, 1–16 (2007).
- Olafsson, J. *et al.* Rate of Iceland Sea acidification from time series measurements. *Biogeosciences* **6**, 2661–2668 (2009).
- Vázquez-Rodríguez, M., Pérez, F. F., Velo, A., Ríos, A. F. & Mercier, H. Observed acidification trends in North Atlantic water masses. *Biogeosciences* **9**, 5217–5230 (2012).
- García-Ibáñez, M. I. *et al.* Ocean acidification in the subpolar North Atlantic: Rates and mechanisms controlling pH changes. *Biogeosciences* **13**, 3701–3715 (2016).
- Orr, J. C. *et al.* Anthropogenic ocean acidification over the twenty-first century and its impact on calcifying organisms. *Nature* **437**, 681–686 (2005).
- Broecker, W. S. & Peng, T. H. *Tracers in the Sea*. (1983). [https://doi.org/10.1016/0016-7037\(83\)90075-3](https://doi.org/10.1016/0016-7037(83)90075-3)
- Feely, R. A., Byrne, R. H., Betzer, P. R., Gendron, J. F. & Acker, J. G. Factors influencing the degree of saturation of the surface and intermediate waters of the North Pacific ocean with respect to aragonite. *J. Geophys. Res.* **89**, 631–640 (1984).
- Subhas, A. V. *et al.* A novel determination of calcite dissolution kinetics in seawater. *Geochim. Cosmochim. Acta* <https://doi.org/10.1016/j.gca.2015.08.011> (2015).
- Roberts, J. M., Wheeler, A. J., Freiwald, A. & Cairns, S. D. Cold-water corals: The biology and geology of deep-sea coral habitats. *Cold-Water Corals Biol. Geol. Deep-Sea Coral Habitats* <https://doi.org/10.1017/CBO9780511581588> (2009).
- Jones, C. G., Lawron, J. H. & Shachak, M. Positive and negative effects of organisms as physical ecosystem engineers. *Ecology* **78**, 1946–1957 (1997).
- Hennige, S. J. *et al.* Self-recognition in corals facilitates deep-sea habitat engineering. *Sci. Rep.* **4**, 1–7 (2014).
- Roberts, J. M. *et al.* Cold-water corals in an era of rapid global change: Are these the deep ocean's most vulnerable ecosystems? in *The Cnidaria, Past, Present and Future* (2016). [https://doi.org/10.1007/978-3-319-31305-4\\_36](https://doi.org/10.1007/978-3-319-31305-4_36)

18. Guinotte, J. M. *et al.* Will human-induced changes in seawater chemistry alter the distribution of deep-sea scleractinian corals?. *Front. Ecol. Environ.* **4**, 141–146 (2006).
19. Davies, A. J., Wisshak, M., Orr, J. C. & Murray Roberts, J. Predicting suitable habitat for the cold-water coral *Lophelia pertusa* (Scleractinia). *Deep. Res. Part I Oceanogr. Res. Pap.* **55**, 1048–1062 (2008).
20. Dullo, W. C., Flögel, S. & Rüggeberg, A. Cold-water coral growth in relation to the hydrography of the Celtic and Nordic European continental margin. *Mar. Ecol. Prog. Ser.* **371**, 165–176 (2008).
21. Sánchez, F. *et al.* Habitat characterization of deep-water coral reefs in La Gavierra Canyon (Avilés Canyon System, Cantabrian Sea). *Deep. Res. Part II Top. Stud. Oceanogr.* **106**, 118–140 (2014).
22. van den Beld, I. M. J. *et al.* Cold-water coral habitats in submarine canyons of the Bay of Biscay. *Front. Mar. Sci.* **4**, 118 (2017).
23. Mostofa, K. M. G. *et al.* Reviews and Syntheses: Ocean acidification and its potential impacts on marine ecosystems. *Biogeosciences* <https://doi.org/10.5194/bg-13-1767-2016> (2016).
24. Milliman, J. D. Production and accumulation of calcium carbonate in the ocean: Budget of a nonsteady state. *Glob. Biogeochem. Cycles* <https://doi.org/10.1029/93GB02524> (1993).
25. Henson, S. A. *et al.* Rapid emergence of climate change in environmental drivers of marine ecosystems. *Nat. Commun.* **8**, 1–9 (2017).
26. Clement, D. & Gruber, N. The eMLR(C\*) method to determine decadal changes in the global ocean storage of anthropogenic CO<sub>2</sub>. *Glob. Biogeochem. Cycles* <https://doi.org/10.1002/2017GB005819> (2018).
27. Pérez, F. F. *et al.* Trends of anthropogenic CO<sub>2</sub> storage in North Atlantic water masses. *Biogeosciences* **7**, 1789–1807 (2010).
28. Pérez, F. F. *et al.* Atlantic Ocean CO<sub>2</sub> uptake reduced by weakening of the meridional overturning circulation. *Nat. Geosci.* **6**, 146–152 (2013).
29. Zunino, P. *et al.* Dissolved inorganic carbon budgets in the eastern subpolar North Atlantic in the 2000s from in situ data. *Geophys. Res. Lett.* **42**, 9853–9861 (2015).
30. Guallart, E. F. *et al.* Trends in anthropogenic CO<sub>2</sub> in water masses of the Subtropical North Atlantic Ocean. *Prog. Oceanogr.* **131**, 21–32 (2015).
31. Carracedo, L. I. *et al.* Role of the circulation on the anthropogenic CO<sub>2</sub> inventory in the North-East Atlantic: A climatological analysis. *Prog. Oceanogr.* **161**, 78–86 (2018).
32. Carracedo, L. I., Pardo, P. C., Flecha, S. & Pérez, F. F. On the mediterranean water composition. *J. Phys. Oceanogr.* **46**, 1339–1358 (2016).
33. Ríos, A. F., Pérez, F. F. & Fraga, F. Long-term (1977–1997) measurements of carbon dioxide in the Eastern North Atlantic: Evaluation of anthropogenic input. *Deep. Res. Part II Top. Stud. Oceanogr.* [https://doi.org/10.1016/S0967-0645\(00\)00182-X](https://doi.org/10.1016/S0967-0645(00)00182-X) (2001).
34. García-Lafuente, J., Sánchez-Román, A., Naranjo, C. & Sánchez-Garrido, J. C. The very first transformation of the Mediterranean outflow in the Strait of Gibraltar. *J. Geophys. Res. Ocean.* <https://doi.org/10.1029/2011JC006967> (2011).
35. Pérez, F. F., Álvarez, M. & Ríos, A. F. Improvements on the back calculation technique for estimating anthropogenic CO<sub>2</sub>. *Deep. Res. Part I Oceanogr. Res. Pap.* [https://doi.org/10.1016/S0967-0637\(02\)00002-X](https://doi.org/10.1016/S0967-0637(02)00002-X) (2002).
36. Huertas, I. E. *et al.* Anthropogenic and natural CO<sub>2</sub> exchange through the strait of gibraltar. *Biogeosciences* **6**, 647–662 (2009).
37. Thorpe, R. B. & Bigg, G. R. Modelling the sensitivity of Mediterranean Outflow to anthropogenically forced climate change. *Clim. Dyn.* <https://doi.org/10.1007/s003820050333> (2000).
38. Kriegler, E. *et al.* Fossil-fueled development (SSP5): An energy and resource intensive scenario for the 21st century. *Glob. Environ. Chang.* **42**, 297–315 (2017).
39. Meinshausen, M. *et al.* The SSP greenhouse gas concentrations and their extensions to 2500. (2019).
40. Lebrato, M. *et al.* Benthic marine calcifiers coexist with CaCO<sub>3</sub>-undersaturated seawater worldwide. *Glob. Biogeochem. Cycles* <https://doi.org/10.1002/2015GB005260> (2016).
41. Baco, A. R. *et al.* Defying dissolution: Discovery of deep-sea scleractinian coral reefs in the North Pacific. *Sci. Rep.* <https://doi.org/10.1038/s41598-017-05492-w> (2017).
42. Form, A. U. & Riebesell, U. Acclimation to ocean acidification during long-term CO<sub>2</sub> exposure in the cold-water coral *Lophelia pertusa*. *Glob. Chang. Biol.* **18**, 843–853 (2012).
43. Maier, C., Hegeman, J., Weinbauer, M. G. & Gattuso, J. P. Calcification of the cold-water coral *Lophelia pertusa* under ambient and reduced pH. *Biogeosciences* **6**, 1671–1680 (2009).
44. Hennige, S. J. *et al.* Short-term metabolic and growth responses of the cold-water coral *Lophelia pertusa* to ocean acidification. *Deep. Res. Part II Top. Stud. Oceanogr.* **99**, 27–35 (2014).
45. Vad, J., Orejas, C., Moreno-Navas, J., Findlay, H. S. & Roberts, J. M. Assessing the living and dead proportions of cold-water coral colonies: Implications for deep-water Marine Protected Area monitoring in a changing ocean. *PeerJ* **2017**, 1–20 (2017).
46. Hennige, S. J. *et al.* Hidden impacts of ocean acidification to live and dead coral framework. *Proc. R. Soc. B Biol. Sci.* **282**, 20150990 (2015).
47. Schönberg, C. H. L., Fang, J. K. H., Carreiro-Silva, M., Tribollet, A. & Wisshak, M. Bioerosion: The other ocean acidification problem. *ICES J. Mar. Sci.* <https://doi.org/10.1093/icesjms/fsw254> (2017).
48. Breitburg, D. *et al.* Declining oxygen in the global ocean and coastal waters. *Science* <https://doi.org/10.1126/science.aam7240> (2018).
49. Durack, P. J. *et al.* Ocean warming from the surface to the deep in observations and models. *Oceanography* **31**, 41–51 (2018).
50. Sloyan, B. M. *et al.* The global ocean ship-base hydrographic investigations program (GO-SHIP): A platform for integrated multidisciplinary ocean science. *Front. Mar. Sci.* **6**, 445 (2019).
51. Clayton, T. D. & Byrne, R. H. Spectrophotometric seawater pH measurements: Total hydrogen ion concentration scale calibration of m-cresol purple and at-sea results. *Deep. Res. Part I* **40**, 2115–2129 (1993).
52. Perez, F. F. & Fraga, F. A precise and rapid analytical procedure for alkalinity determination. *Mar. Chem.* [https://doi.org/10.1016/0304-4203\(87\)90037-5](https://doi.org/10.1016/0304-4203(87)90037-5) (1987).
53. Velo, A. *et al.* CARINA data synthesis project: PH data scale unification and cruise adjustments. *Earth Syst. Sci. Data* <https://doi.org/10.5194/essd-2-133-2010> (2010).
54. Olsen, A. *et al.* The global ocean data analysis project version 2 (GLODAPv2)—An internally consistent data product for the world ocean. *Earth Syst. Sci. Data* <https://doi.org/10.5194/essd-8-297-2016> (2016).
55. Olsen, A. *et al.* GLODAPv2.2019: An update of GLODAPv2. *Earth Syst. Sci. Data Discuss.* <https://doi.org/10.5194/essd-2019-66> (2019).
56. Van Heuven, S., Pierrot, D., Rae, J. W. B., Lewis, E. & Wallace, D. W. R. CO2SYS v 1.1, MATLAB program developed for CO<sub>2</sub> system calculations. ORNL/CDIAC-105b. Carbon Dioxide Inf. Anal. Center, Oak Ridge Natl. Lab. U.S. DoE, Oak Ridge, TN. (2011). <https://doi.org/10.1017/CBO9781107415324.004>
57. Mehrbach, C., Culberson, C. H., Hawley, J. E. & Pytkowicz, R. M. Measurement of the apparent dissociation constants of carbonic acid in seawater at atmospheric pressure. *Limnol. Oceanogr.* <https://doi.org/10.4319/lo.1973.18.6.0897> (1973).
58. Dickson, A. G. & Millero, F. J. A comparison of the equilibrium constants for the dissociation of carbonic acid in seawater media. *Deep Sea Res. Part A Oceanogr. Res. Pap.* [https://doi.org/10.1016/0198-0149\(87\)90021-5](https://doi.org/10.1016/0198-0149(87)90021-5) (1987).
59. Mucci, A. The solubility of calcite and aragonite in seawater at various salinities, temperatures, and one atmosphere total pressure. *Am. J. Sci.* <https://doi.org/10.2475/ajs.283.7.780> (1983).

60. Orr, J. C., Epitalon, J. M., Dickson, A. G. & Gattuso, J. P. Routine uncertainty propagation for the marine carbon dioxide system. *Mar. Chem.* <https://doi.org/10.1016/j.marchem.2018.10.006> (2018).
61. Millero, F. J., Feistel, R., Wright, D. G. & McDougall, T. J. The composition of standard seawater and the definition of the reference-composition salinity scale. *Deep. Res. Part I Oceanogr. Res. Pap.* <https://doi.org/10.1016/j.dsr.2007.10.001> (2008).
62. Raven, J. *et al.* Ocean acidification due to increasing atmospheric carbon dioxide. *R. Soc.* **5**, 60 (2005).
63. Vázquez-Rodríguez, M. *et al.* Anthropogenic carbon distributions in the Atlantic Ocean: Data-based estimates from the Arctic to the Antarctic. *Biogeosciences* **6**, 439–451 (2009).
64. Freiwald, A. *et al.* Global distribution of cold-water corals (version 5.0). Fifth update to the dataset in Freiwald *et al.* (2004) by UNEP-WCMC. (UN Environment World Conservation Monitoring Centre, Cambridge, 2017).
65. Ríos, A. F., Pérez, F. F. & Fraga, F. Water masses in the upper and middle North Atlantic Ocean east of the Azores. *Deep Sea Res. Part A Oceanogr. Res. Pap.* [https://doi.org/10.1016/0198-0149\(92\)90093-9](https://doi.org/10.1016/0198-0149(92)90093-9) (1992).
66. Lherminier, P. *et al.* Transports across the 2002 Greenland-Portugal Ovide section and comparison with 1997. *J. Geophys. Res. Ocean.* **112**, 1–20 (2007).

## Acknowledgements

For this work M. Fontela was funded by the Spanish Ministry of Economy and Competitiveness (BES-2014-070449) supported by the Spanish Government and co-funded by the Fondo Europeo de Desarrollo Regional 2007–2012 (FEDER) and by Portuguese national funds from FCT—Foundation for Science and Technology through project UID/Multi/04326/2019 and CEECINST/00114/2018. F.F. Pérez was supported by the BOCATS Project (CTM2013-41048-P) and ARIOS project (CTM2016-76146-C3-1-R) both co-funded by the Spanish Government and the Fondo Europeo de Desarrollo Regional (FEDER). This project has received funding from the European Union's Horizon 2020 research and innovation programme under grant agreement No 820989 (project COMFORT, Our common future ocean in the Earth system—quantifying coupled cycles of carbon, oxygen, and nutrients for determining and achieving safe operating spaces with respect to tipping points). We thank Evan Edinger and Mario Lebrato for their constructive and useful review that greatly helped to improve the paper.

## Author contributions

M.F., F.F.P. and L.I.C. wrote the manuscript. M.F. prepared all the figures. M.F. and F.F.P. analyzed the data. M.F., F.F.P., L.I.C., X.A.P., A.V., M.I.G-I. and P.L. have contributed to the acquisition of data, have participated in the results discussion and have reviewed the manuscript and supporting information.

## Competing interests

The authors declare no competing interests.

## Additional information

**Supplementary information** is available for this paper at <https://doi.org/10.1038/s41598-020-71793-2>.

**Correspondence** and requests for materials should be addressed to M.F.

**Reprints and permissions information** is available at [www.nature.com/reprints](http://www.nature.com/reprints).

**Publisher's note** Springer Nature remains neutral with regard to jurisdictional claims in published maps and institutional affiliations.



**Open Access** This article is licensed under a Creative Commons Attribution 4.0 International License, which permits use, sharing, adaptation, distribution and reproduction in any medium or format, as long as you give appropriate credit to the original author(s) and the source, provide a link to the Creative Commons licence, and indicate if changes were made. The images or other third party material in this article are included in the article's Creative Commons licence, unless indicated otherwise in a credit line to the material. If material is not included in the article's Creative Commons licence and your intended use is not permitted by statutory regulation or exceeds the permitted use, you will need to obtain permission directly from the copyright holder. To view a copy of this licence, visit <http://creativecommons.org/licenses/by/4.0/>.

© The Author(s) 2020